Measurements of the Movement, Concentration and Dimensions of Clouds Resulting from Instantaneous Point Sources[1]

P. W. NICKOLA

Battelle Memorial Institute, Pacific Northwest Laboratory, Richland, Wash.

(Manuscript received 23 February 1971, in revised form 25 May 1971)

ABSTRACT

Puffs of the inert gas ^{85}Kr were released at the surface level and were permitted to drift through a three-dimensional grid of Geiger counter sensors extending to a height of 21 m and to a distance of 800 m. Concentrations were recorded as a series of 4.8-sec duration mean concentrations for each of the 64 sensors. Data specifying the effective speed, the effective height, the magnitude of short-period concentrations, the magnitude of crosswind and downwind concentration integrations, and the dimensions of puffs are reported. It was found that: 1) the speed with which a puff reached a 1.5 m elevation field sensor increased with distance from the source (or with travel time); 2) at the 1.5 m elevation, peak values of short-period concentration, exposure, and crosswind integrated concentration increased with increasing atmospheric stability; 3) regardless of the atmospheric stability, puff dimensions along a downwind axis exceeded those along a crosswind axis, and the crosswind dimension exceeded the vertical; 4) for a given distance, the ratio of crosswind to downwind dimensions decreased as atmospheric stability increased; 5) the ratio of crosswind to downwind puff dimensions increased with distance (or time) in an unstable atmosphere but decreased slightly in stable atmospheres; 6) the ratio of vertical to downwind puff dimensions decreased with distance (or time) regardless of stability; and 7) the effects of stability on puff dimensions were best shown when dimensions were considered as a function of time rather than distance from the source.

1. Introduction

Field measurements aimed at the description of puffs resulting from instantaneous point sources have received little attention when compared to the efforts expended in the definition of plumes resulting from continuous point sources. This emphasis on plumes stems partially from concern with the great number of industrial stacks which, by design, emit pollutants on a more or less continuous basis. In contrast, puffs of pollutants are associated with infrequent and accidental releases—explosions or rocket launch-pad accidents, for example.

A second reason for the lack of field investigation of instantaneous point sources is that generation and measurement are technically more difficult for puffs than for longer period releases. A plume may be considered as the addition of an infinite number of overlapping puffs. Sections through any location in a plume will reveal dimensions larger than the dimensions of any of the individual puffs contributing to the composite plume. Thus, a finer spacing on a measurement grid is required to adequately investigate and define puff dimensions. Conversely, the crosswind extent of sampling must be essentially as great as required with longer period releases since the mean wind direction in which a puff is "imbedded" is no more controllable or predictable for the puff than is the case for a plume.

Additionally, equations specifying puff concentration incorporate a term which defines the downwind as well as the crosswind vertical and horizontal dimensions. A downwind dimension is not applicable in continuous plume considerations. Thus, an additional measurement capability is required in field investigations dealing with puffs.

Finally, it has proven far easier to simulate continuous releases than instantaneous or quasi-instantaneous releases using point source dispersal methods. Plumes have been generated by such methods as atomizing liquids, releasing compressed gases from bottles, and injecting small particulates into air streams. Attempts at generation of "instantaneous" sources, however, have frequently involved use of continuous tracer generation techniques, but over short intervals of time, i.e., the "puff" in these cases is in reality a short plume. One problem here is in the release of enough tracer for adequate detection.

An excellent review of theory and of experiments dealing with instantaneous point sources is given by Gifford in Chapter 3 and by Islitzer and Slade in Chapter 4 of *Meteorology and Atomic Energy, 1968* (U. S. Atomic Energy Commission, 1968).

A series of eight puff releases on the Battelle-Northwest field grid at the U. S. Atomic Energy Commission's Hanford project has afforded an opportunity to observe diffusing puffs in greater detail than has

[1] This paper is based on work performed under U. S. Atomic Energy Commission Contract AT(45-1)-1830.

heretofore been possible. The purpose of this paper is to present data and data analyses resulting from the release of these instantaneous point sources.

2. The Hanford ^{85}Kr atmospheric tracer technique

The atmospheric tracer technique developed at Hanford employs the inert radioactive gas ^{85}Kr as the tracer. Ludwick *et al.* (1968) emphasized instrumentation in reporting development of the technique. All data generated to date through use of this system as well as a description of the system itself have been compiled by Nickola *et al.* (1970a), while a less detailed description of the system has been published by Nickola *et al* (1970b). Results from use of this system have been reported by Nickola and Ludwick (1968), by Ramsdell and Hinds (1971), and by several contributions in the most recent Pacific Northwest Laboratory (1970) annual report to the Division of Biology and Medicine, U. S. Atomic Energy Commission.

The field grid employed with ^{85}Kr release is shown schematically in Fig. 1. Puffs were released at the center of the field grid by crushing vials containing the tracer in a guillotine-like device. The vials were crushed at ground level. The gas in each ampule had been sealed at near atmospheric pressure so as to minimize the initial volume and hence to better simulate an instantaneous point source. Although no direct measurement was made of initial puff size, it is estimated that puff diameters were ~1 m. Inasmuch as the krypton tracer is an inert gas, depletion of the puff by such processes as chemical reaction and deposition were avoided. As a puff moved downwind, it was detected by a series of 64 halogen-quenched Geiger-Müller tubes located on concentric arcs 200 and 800 m from the source point. As Fig. 1 shows, 20 of these detectors, 1.5 m above the ground, were spaced at 2° intervals on each of the sampling arcs. The remaining 24 samplers were mounted on six towers, three towers to each arc.

Information from these detectors was relayed by coaxial cables to a 4096 address memory which was programmed to accept data simultaneously from the 64 detectors for 64 time increments. After each 4.8 sec of simultaneous sampling of the 64 detectors, a timed automatically advanced count accumulation to the next 64 memory channels. The process was repeated until information accumulation completely filled the 64 time increments of the memory. The memory was then read to a magnetic tape, which provided input for a device which, in turn, provided a photographic reproduction of the counts accumulated in each channel. When field count rates remained above background at the end of the 64 time increments, the memory was cleared as soon as the data were read to the magnetic tape, and memory accumulation and automatic stepping were resumed. The dump and reactivate procedure usually required about 45 sec.

Terrain in the area of the ^{85}Kr field diffusion grid is relatively flat. The extremes in elevation on the grid differ by only 20 ft.

Vegetation is primarily sagebrush and steppe grasses.

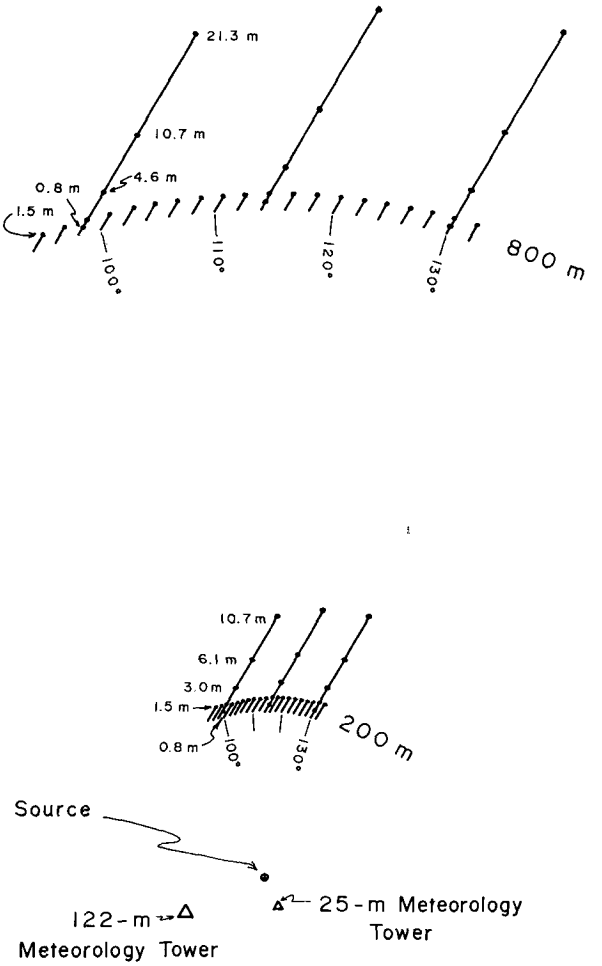

FIG. 1. Schematic representation of ^{85}Kr field grid.

3. Data

Table 1 presents some general information concerning the eight puff releases. The definition of symbols used in Table 1 and elsewhere in this report are listed in an Appendix. In Table 1, the tests are listed in order of decreasing atmospheric stability as indicated by the Richardson number.

The primary output from the ^{85}Kr tracer system is in the form of a distribution of tracer concentration with respect to time and direction from the source for an elevation 1.5 m above the surface, and at distances of 200 m and 800 m from the source. In addition, the distribution of tracer concentration with respect to time and height above the surface is determined for the six tower locations. [Nickola *et al.* (1970b) gives examples of these primary data.] These data may be used to prepare distributions of puff concentrations in the x, y and z

TABLE 1. Puff releases: times and accompanying meteorology.

Test	Release Date (1967)	Release Time (PST)	$\bar{u}_{1.5\,m}$ to 200 m (m sec^{-1})	$\bar{u}_{1.5\,m}$ to 800 m (m sec^{-1})	During puff travel to 800 m σ_θ (deg)	During puff travel to 800 m σ_u (m sec^{-1})	Ri	Qualitative stability
P7	24 October	1052	5.1	4.6	9.1	0.91	−0.16	Unstable
P4	17 October	0838	4.9	4.9	6.8	0.82	−0.05	Neutral
P6	23 October	1130	7.3	7.3	5.3	1.25	−0.04	Neutral
P3	17 October	0738	4.0	4.2	5.2	0.79	−0.03	Neutral
P5	23 October	1053	8.0	8.0	7.4	1.36	−0.02	Neutral
P8	8 November	0602	1.4	1.5	7.3	0.27	0.07	Stable
P1	18 August	0312	2.4	—	—	—	0.12	Stable
P2	14 September	2300	1.2	1.2	4.8	0.12	0.13	Stable

directions. Examples of these distributions are given in Figs. 2, 3 and 4 for Tests P7 (unstable atmosphere) and P8 (stable atmosphere).

Fig. 2 presents distributions of exposure at an elevation of 1.5 m along arcs at distances of 200 and 800 m from the source. Data of this nature are not uncommon, and are generally obtained through use of a collector (such as a filter) which has no time-resolution capability, but which simply integrates concentration over the entire time of its exposure. In the ^{85}Kr technique, exposure (a time-integrated concentration) is obtained for a given location by summing all short-period concentrations observed at that location.

Fig. 3 gives exposure vs height curves at selected azimuths for field tests P7 and P8. The solid curves pass through measured data points. The dotted portions of the curves are extrapolations above the topmost sampling levels. The dashed "deduced" curves will be discussed later in this paper. Vertical profiles of exposure are less commonly reported in diffusion literature since mounting platforms such as towers or balloons are required to support sampling equipment. The use of permanently mounted sensors with the ^{85}Kr system permits determination of vertical profiles of exposure in exactly the same way as with the ground-level sensors.

Fig. 4 presents crosswind summed concentrations vs

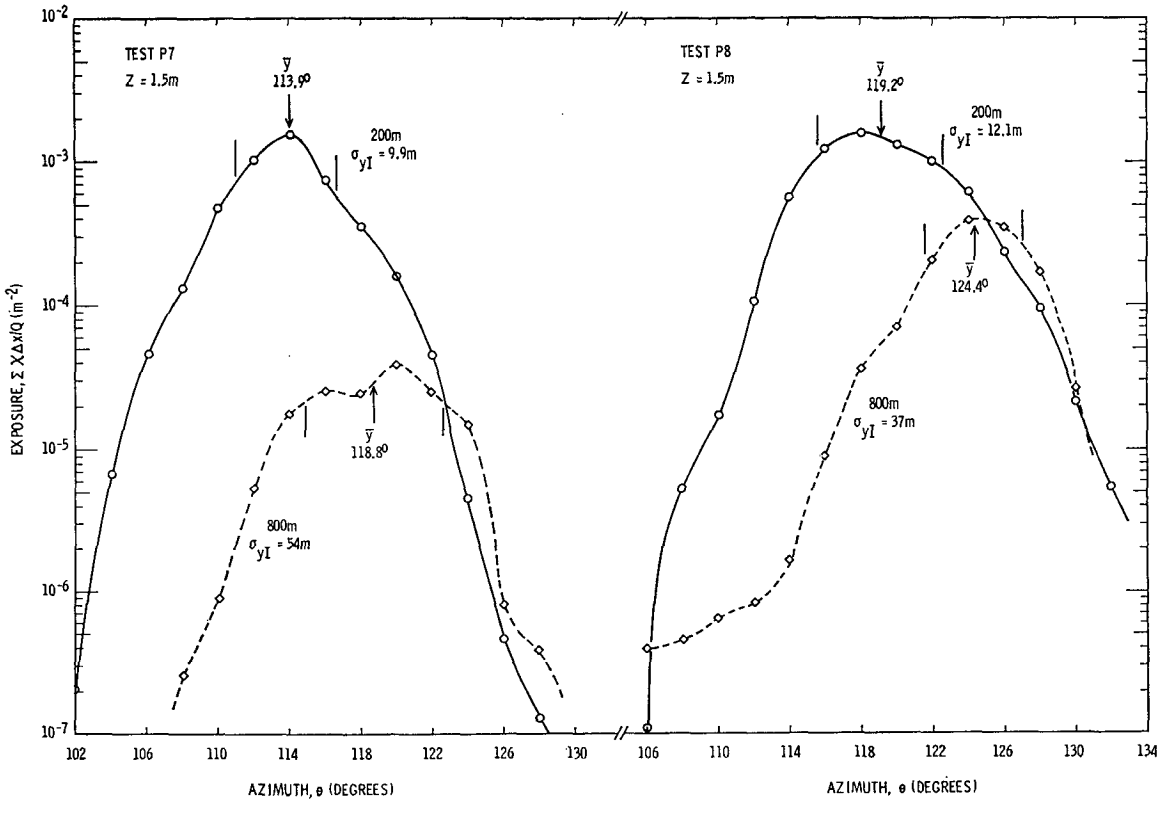

FIG. 2. Exposure vs azimuth for field tests P7 and P8.

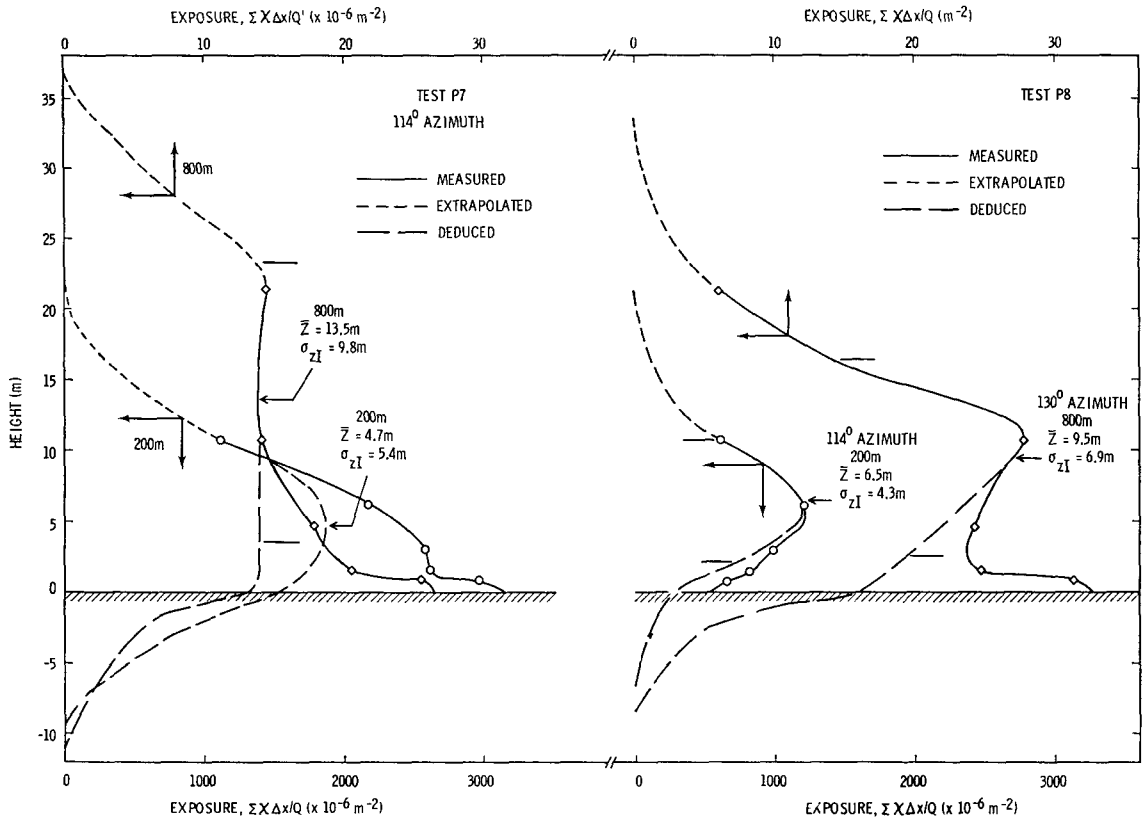

FIG. 3. Exposure vs height for selected azimuths for field tests P7 and P8.

elapsed time following puff release. Data are for 1.5 m sensors. Although measurement of tracer concentration vs time has been attempted in the past, it has not been accomplished with as detailed a sampler array as is reported here. Further, the author is unaware of any other such measurements involving puff releases. These distributions permit estimation of downwind dimensions of diffusing puffs.

Of the eight puffs released, only six remained sufficiently within the bounds of the array of sensors to permit crosswind or downwind summing of exposures as is presented in Figs. 2 and 4. The tracer extended above the topmost sampling level on one or more towers during each puff release. This fact restricted the usefulness of the tower data, although extrapolations from observed data points were made in order to estimate vertical plume dimensions.

Unfortunately, during test P2 the krypton field sensors were inactivated prior to the completion of tracer passage at 800 m. Since this test was carried out under the most stable atmospheric conditions of the whole series, a relatively large extrapolation was undertaken in order to permit incorporation of the 800 m data points in this study. This extrapolation suggests that about 10% of the tracer passed the 800 m arc subsequent to data collection.

During these prototype tests (with the exception of test P1), the area upwind of the source was less than perfect in terms of the clear fetch desired in an ideal diffusion study. A flatbed trailer about 6 m in length was parked about 4 m upwind of the source location. Several boxlike items were spaced on the trailer. Overall, a lattice-like cross section of 8–10 m^2 was presented to the wind approaching the source, and undoubtedly caused some wake effects in the vicinity of the source.

It should be stressed that the data primarily employed in this study were collected at an elevation of 1.5 m above the surface. Unless stated otherwise, the parameters generated in this paper apply to this 1.5 m level—a level that approximates the breathing level of man. It would be fortuitous if this level were the elevation of maximum concentrations for any of the sampling arcs for any test. Although vertical sampling was undertaken on towers, the distance between these towers was too great to permit reasonable estimates of flux passing through vertical cylindrical surfaces centered on the source point. In view of the fact that the puff was released directly at the earth's surface, it would not be unreasonable to assume that maximum concentrations were "near" the 1.5 m level. In many cases, however, the tower data showed greater concentrations at elevations above 1.5 m. And so, to close the paragraph as it began, the data presented in this study do *not* result

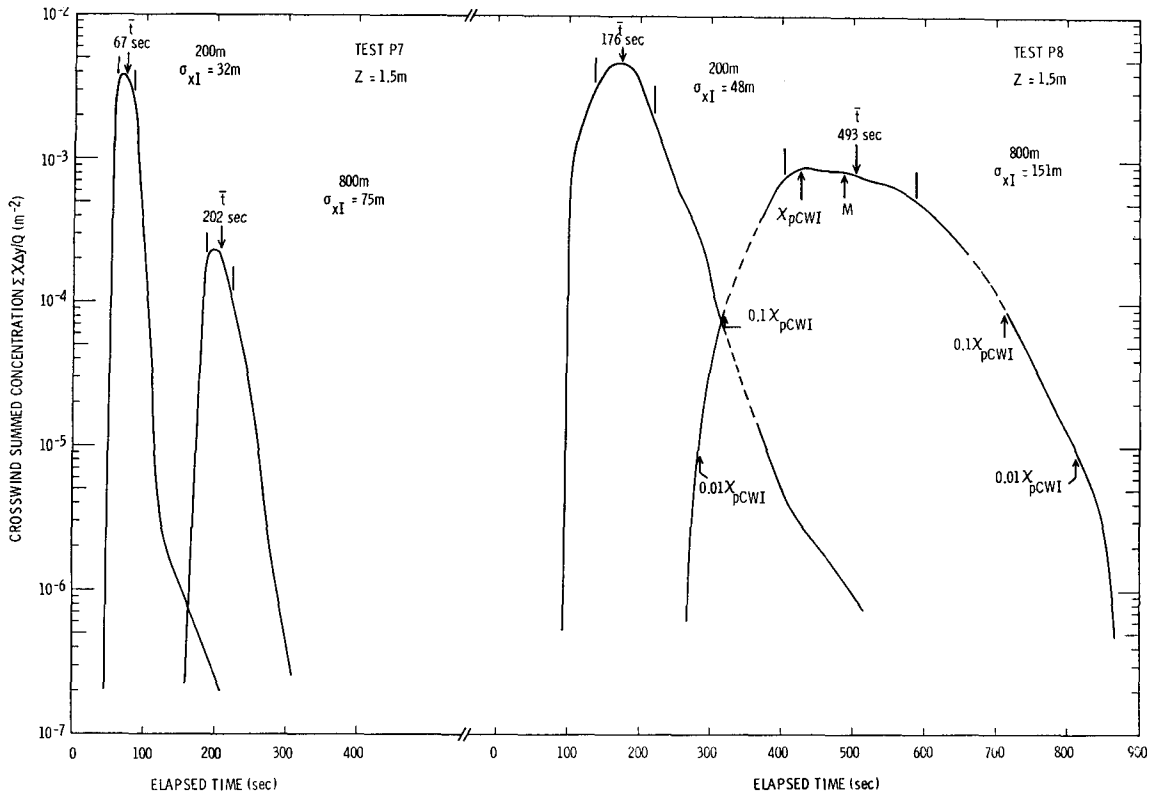

FIG. 4. Crosswind summed concentration vs elapsed time since puff release. Multiplication of elapsed time by an appropriate transport speed converts the time scale to a length scale extending radially from the source.

from axial concentrations, but from measurements made at the 1.5 m elevations.

4. Puff movement

Since the distance from the source to each field detector was known, and since the time of arrival of tracer was recorded, the speed with which the tracer moved from source to sensor was easily computed. This speed and the associated height (determined from wind profiles taken on a 25 m tower instrumented at six levels) are termed the effective transport speed u_e and the effective transport height z_e, respectively. Values of u_e and z_e can be computed for various identifiable portions of each puff. For instance, the mean times $\bar{t}$ for the crosswind summed concentration distributions are noted on Fig. 4. These mean times may be used to specify puff passage at each arc.

Values of $\bar{t}$ and their associated u_e and z_e values are listed in Table 2. At 200 m it should be noted that u_e was always less than the wind speed measured at the

TABLE 2. Effective transport speeds and heights for concentration measurements made at an elevation of 1.5 m.

		200 m			800 m			Effective transport height z_e											
			@t			@$\bar{t}$		200 m						800 m					
								Leading edge				Trailing edge		Leading edge				Trailing edge	
Test	Ri	$\bar{t}$ (sec)	u_e (m sec^{-1})	z_e (m)	$\bar{t}$ (sec)	u_e (m sec^{-1})	z_e (m)	@0.01 χ_{pCWI}	@0.1 χ_{pCWI}	@χ_{pCWI}	@M	@0.1 χ_{pCWI}	@0.01 χ_{pCWI}	@0.01 χ_{pCWI}	@0.1 χ_{pCWI}	@χ_{pCWI}	@M	@0.1 χ_{pCWI}	@0.01 χ_{pCWI}
P7	−0.16	67	3.0	0.5*	202	4.0	0.9	1.0	0.9	0.6*	0.5*	0.3*	0.3*	3.0	1.8	1.0	0.9	0.6*	0.5*
P4	−0.05	43**	4.7**	1.3**	140*	5.7**	2.8**	—	—	—	1.3**	—	—	—	—	—	2.8**	—	—
P6	−0.04	42	4.7	0.5*	122	6.6	1.1	1.6	1.4	0.6*	0.5*	0.3*	0.2*	5.0	3.0	1.3	1.1	0.7*	0.5*
P3	−0.03	81	2.5	0.5*	215	3.7	1.1	1.1	1.1	0.6*	0.5*	0.3*	0.3*	4.5	3.0	1.3	1.2	0.6*	0.5*
P5	−0.02	39	5.1	0.5*	113	7.1	1.1	1.8	1.4	0.7*	0.5*	0.3*	0.2*	4.6	3.2	1.2	1.1	0.6*	0.5*
P8	0.07	176	1.1	1.0	493	1.6	1.8	5.6	4.2	1.1	1.0	0.5*	0.3*	8.8	6.9	2.5	1.9	0.6*	0.4*
P2	0.13	406	0.49	0.5*	833	0.96	1.1	1.2	1.1	0.6*	0.5*	0.4*	0.3*	3.1	2.7	1.3	1.2	0.6*	0.5*

* Based on wind profile extrapolated below lowest anemometer height of 0.75 m. Other anemometers are at 1.5, 3, 6, 12 and 24 m.
** Estimate due to truncated crosswind distribution.
@ Signifies "at."

sampling height ($z=1.5$ m); consequently, z_e was always between the sampling height and the release height ($z\approx 0$). The upward mixing of the tracer was evidenced by the fact that in all cases z_e values were greater at 800 than at 200 m. For tests P4 and P8, the mean of the tracer reaching 800 m was actually transported at a speed and height above the 1.5 m sampling level.

Perhaps a more meaningful way of considering z_e is as a function of travel time rather than distance. This procedure reduces the effects of different wind speed for different tests. Fig. 5 shows z_e as a function of $\bar{t}$. The stable tests (P2, P8) and the unstable test (P7) generally have lower z_e values than do the neutral tests. The rate of change of z_e is lowest for unstable test P7 and highest for the most stable test P2. However, stable P8 also shows a relatively low rate of change of z_e. These few field releases do not suggest a strong dependency of z_e on atmospheric stability.

Table 2 also lists z_e values for locations in the puff other than at $\bar{t}$. Effective transport heights for the median (M) of the distribution as well as the peak 4.8-sec duration crosswind integrated concentration ($\chi_{p\text{CWI}}$) are presented. In skewed distributions as illustrated at the right in Fig. 4, times of $\chi_{p\text{CWI}}$ and M occur at a time prior to $\bar{t}$. However, the difference in t is so small that Table 2 shows nearly identical values of z_e for $\bar{t}$, M and $\chi_{p\text{CWI}}$.

Values of z_e for leading and trailing portions of the puff are also presented. The concentrations selected as possible definitions of the "edges" of the puffs are 0.1 $\chi_{p\text{CWI}}$ and 0.01 $\chi_{p\text{CWI}}$.

Table 2 reveals, then, the heights at which the measured wind indicated the arrival and departure of the tracer from either 200 or 800 m. For example, during test P8 an anemometer exposed at an elevation of 8.8 m would have recorded the speed with which tracer would first be detected at 800 m. An anemometer at an elevation of 0.4 m would have revealed the speed at which the trailing edge of the plume reached 800 m. Note that z_e values for the trailing edges of the seven tabulated puffs have small scatter as compared to z_e values for the leading edges.

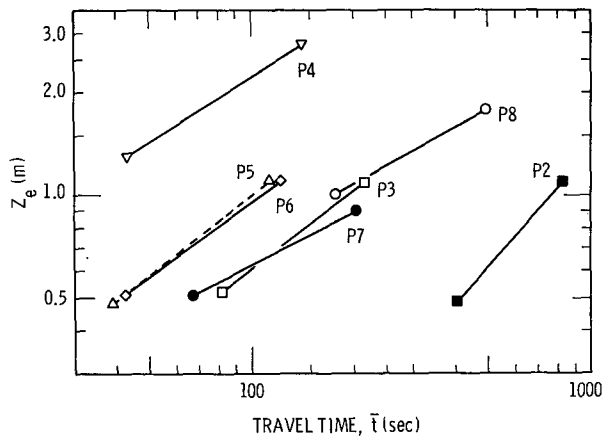

FIG. 5. Effective transport height vs mean travel time.

Perhaps it should be reemphasized that the concentration measurements from which Table 2 was developed were made at an elevation of 1.5 m. Although perhaps the centroid was not far removed, this 1.5 m level was likely not the elevation of the centroid of the moving puff. Further, the computed effective speeds and heights would undoubtedly be considerably higher for releases above the surface level.

It was noted, during the low wind speed and stable atmosphere of test P2, that tracer was in evidence at a distance 200 m from the source for a period in excess of 15 min.

5. Concentration measurements

Table 3 again lists the puff release experiments in order of increasing stability. This table also lists (for the 1.5-m level) normalized values of peak exposure, E_p/Q; of peak crosswind integrated concentration, $\chi_{p\text{CWI}}/Q$; and of peak short-period (4.8-sec duration) concentration, χ_p/Q. It can be seen that all these quantities tend to increase with increasing stability. Generally the rate of decrease of these quantities with distance is greater for the less stable experiments.

TABLE 3. Maximum values of exposure, crosswind integrated concentration, and short-period concentration observed at an elevation of 1.5 m.

		E_p/Q		$\chi_{p\text{CWI}}/Q$		χ_p/Q		Tracer in 1–2 m layer	
Test	Ri	200 m ($\times 10^{-6}$m^{-2})	800 m ($\times 10^{-6}$m^{-2})	200 m ($\times 10^{-6}$m^{-2})	800 m ($\times 10^{-6}$m^{-2})	200 m ($\times 10^{-6}$m^{-3})	800 m ($\times 10^{-6}$m^{-3})	200 m (%)	800 m (%)
P7	−0.16	1600	38	3900	240	21	0.25	3.2	0.4
P4	−0.05	1200*	130*	—	—	11*	0.43*	—	—
P6	−0.04	1900	120	5300	720	23	0.68	4.9	1.4
P3	−0.03	680	200	3100	580	11	0.92	2.5	1.5
P5	−0.02	1700	150	4500	690	19	0.78	4.1	1.5
P8	0.07	1600	400	4800	920	19	1.21	4.8	2.6
P1	0.12	—	—	—	—	16	—	—	—
P2	0.13	2100	610	6500	1640	44	4.64	6.7	7.0

* Tabulated value may be low since it was taken at the edge of a truncated distribution.

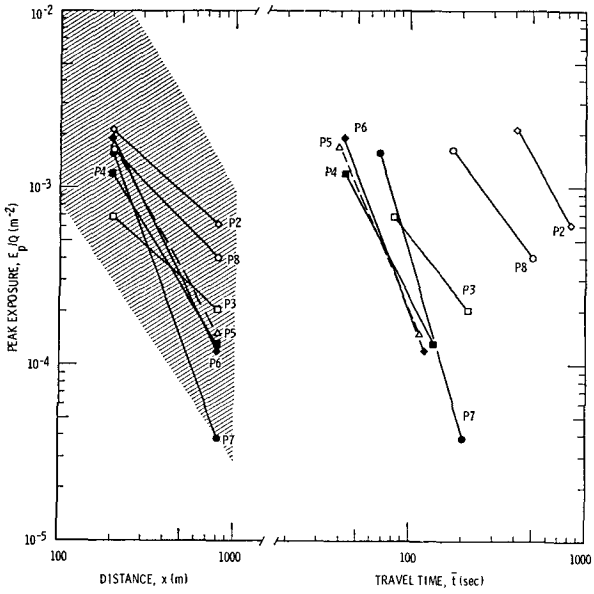

FIG. 6. Peak exposure vs distance and travel time.

A comparison of E_p/Q values with $\chi_{p\mathrm{CWI}}/Q$ reveals that E_p/Q (a downwind integration) decreases at a more rapid rate than $\chi_{p\mathrm{CWI}}/Q$ (a crosswind integration) during unstable test P7. The opposite is true during stable tests P2 and P8. However, the absolute value of $\chi_{p\mathrm{CWI}}/Q$ was greater than E_p/Q for all tests, at least to a distance of 800 m. Thus, a person moving (at a rapid rate when compared to the wind speed) directly directly up or downwind through the middle of a puff could expect to breathe a smaller amount of contaminant than his friend who dashed through the center of the puff in a crosswind direction.

Normalized peak exposure vs distance from source is plotted at the left in Fig. 6. These peak exposures do not differ greatly for those generally accepted for plumes. Stratification by stability is not obvious at 200 m (where, perhaps, the effect of the previously mentioned wake at the source is more significant), but stratification into stable, neutral and unstable categories is seen at the 800 m distance. The shaded area embraces the range of values from quasi-instantaneous sources released at Edwards Air Force Base, Calif. (Taylor, 1965) and at Dugway Proving Grounds, Utah (Cramer *et al.*, 1964) as presented in *Meteorology and Atomic Energy, 1968* (U. S. Atomic Energy Commission, 1968). Tracer release and measurements of concentration were made near the surface in the referenced studies.

In the right-hand portion of Fig. 6, peak exposure is examined on the basis of travel time $\bar{t}$ rather than distance. This time dependency approach reveals a better separation of the stable experiments (P2 and P8) from the others, but requires an extrapolation to about 300 sec before the unstable test P7 shows a smaller E_p/Q than all the neutral tests. These data suggest that peak exposures at 300 sec for the stable tests are two or more orders of magnitude higher than those for the unstable test.

Fig. 7 presents peak short-period (4.8-sec) concentration vs distance and time, i.e., the elapsed time required for the observed χ_p values. The data group reasonably well with stability as in Fig. 6, and again the use of time accentuates the effects of a stable atmosphere. Plotting of either $\chi_p\bar{u}_e/Q$ or $\chi_p\bar{u}_{1.5\ \mathrm{m}}/Q$ vs distance greatly reduces or eliminates the separation of data on the basis of stability. Plotting of these wind-normalized χ_p's vs travel time results in a graph whose stratification is essentially identical to the right-hand graph in Fig. 7.

If it is assumed that the concentration measurements made at the 1.5 m elevation are representative of the slice of atmosphere between 1.0 and 2.0 m, the fraction of the entire mass of tracer passing 200 and 800 m within that 1 m thick slice can be computed. The last two columns of Table 3 present these fractions. The suppression of vertical motion by the more stable atmospheres is evident from examination of these columns, particularly at 800 m. At 800 m, the mass of material transported at this low-level layer during stable test P2 was 18 times as great as during unstable test P7.

6. Puff dimensions

Consider a cylindrical coordinate system centered at the tracer source with coordinates of horizontal distance x, elevation z, and azimuth angle θ. A dense three-dimensional network of samplers would permit direct measurement of tracer concentration distribution in any θ, z, or (curved) x plane. The array of samplers

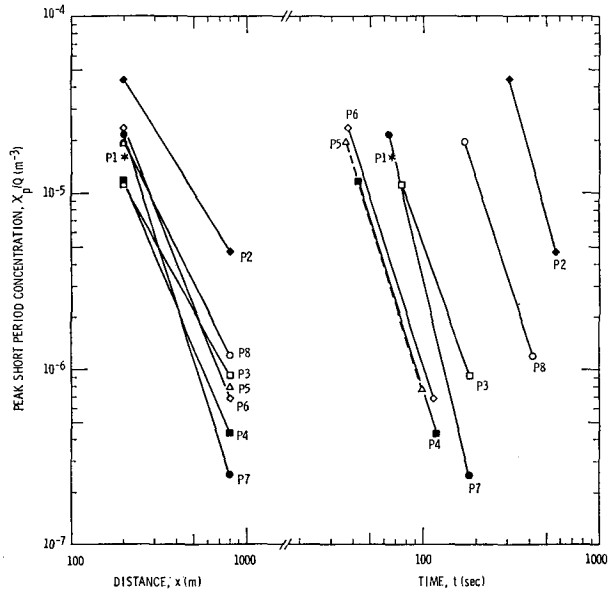

FIG. 7. Peak short-period (4.8-sec duration) concentration vs distance and travel time.

depicted in Fig. 1 is relatively dense in terms of atmospheric sampling grids, but certainly is inadequate for completely defininining concentration distribution in a puff of, say, 10 m in diameter. Spacing between sampling arcs is 600 m, and between towers is 56 m at the 200 m arc and 224 m at the 800 m arc.

Since none of the observed puffs intersected more than two towers at a given distance from the source, our knowledge of the distribution of concentration with time on a z plane other than $z=1.5$ m is minimal.

However, the distribution of concentration with time is well described for the plane $z=1.5$ m. Fig. 4 shows the result of crosswind integration of this distribution for tests P7 and P8. If it is assumed that the u_e values given in Table 2 for $\bar{t}$ are applicable during an entire puff passage at a given distance and at the 1.5 m elevation, the abscissa of Fig. 4 may be converted to units of distance, i.e., $x=u_e\bar{t}$. The standard deviation of the distribution of ^{85}Kr in the x direction, $\sigma_{x\mathrm{I}}$, can then be computed. The unlabelled tics on the curves of Fig. 4 show the location of the standard deviations of the time distributions. The converted values of $\sigma_{x\mathrm{I}}$ in meters are also listed on the figure. The Δy employed in the definition of crosswind summed concentration in Fig. 4 is the spacing between samplers along an arc. For each distance, the spacing is converted from units of degrees to units of distance.

The downwind integration of concentration with time results in exposure as is graphed in Fig. 2. The Δx employed in computing ordinate values results from employment of u_e, i.e., $\Delta x=u_e\Delta t$, where Δt is the 4.8-sec time increment over which short-term χ's were successively measured. Values of $\sigma_{y\mathrm{I}}$ computed from these exposure distributions are listed on Fig. 2 for tests P7 and P8.

The possibility exists of computing $\sigma_{x\mathrm{I}}$ and $\sigma_{z\mathrm{I}}$ from tower data for the plane $\theta=98°$, 114° or 130°. The procedure is analogous to that used with the $z=1.5$ m plane except that the marginal distributions are now functions of x and z, instead of x and y, and the u_e values employed are derived from concentration data at the appropriate tower.

Because of the relatively few towers and their limited vertical extent, it was not possible to obtain tracer distributions and associated $\sigma_{x\mathrm{I}}$ and $\sigma_{z\mathrm{I}}$ values for all tests and distances. Further, in all cases where tower data were used, some extrapolation of measured concentration above the tops of the towers was necessary. The dotted portions of the curves on Fig. 3 are such extrapolations. Considering all tests, the area under the extrapolated portions of the curves varied from 3 to 11% at 200 m, and from 4 to 29% at 800 m.

Another difficulty arose in working with tower data. If the puffs had resulted from elevated releases, a bell-shaped vertical distribution of concentration would have been expected. If perfect surface reflection had taken place with these ground level releases, a half-bell shape could have been anticipated. However, most measurements did not disclose such half-bell distributions. As a result, $\sigma_{z\mathrm{I}}$ values were computed by two methods. The first method employed the data directly and assumed total perfect reflection. This technique was used only in cases where the vertical profile of exposure approached the half-bell shape. The curve for test P7 at 200 m (depicted on Fig. 3) is such a curve.

It was felt that if the perfect reflection assumption had been used with many of the vertical distributions, significance of a standard deviation of the distribution would have been minimal. The distribution shown on Fig. 3 for test P8 at 200 m is an example. In an attempt to eliminate the interferring effects of the surface on the vertical distribution, a second technique was employed in generating $\sigma_{z\mathrm{I}}$ values. In all cases where a reasonable amount of tower data were available, the observed exposures were redistributed into a virtual distribution extending below ground level before computation of $\sigma_{z\mathrm{I}}$'s was begun. The dashed "deduced" curves of Fig. 3 are examples of such distributions. In constructing these deduced curves, the assumption of partial reflection of tracer was made. The exposure at ground level was assumed to be half the observed value, and exposures were then subtracted from a given level above the surface and added to a like level below the surface on a trial-and-error basis until a curve with a reasonably smooth bell-like shape was obtained. This approach is admittedly subjective, but seemed a better technique of approaching $\sigma_{z\mathrm{I}}$ than by merely assuming perfect reflection in all cases regardless of the profile.

Table 4 presents values of $\sigma_{x\mathrm{I}}$, $\sigma_{y\mathrm{I}}$ and $\sigma_{z\mathrm{I}}$. For the four tests in which a range is given for $\sigma_{z\mathrm{I}}$ at 200 m, the larger value results from the total reflection assumption. The smaller of the dual values of $\sigma_{z\mathrm{I}}$, and all cases in which only a single value of $\sigma_{z\mathrm{I}}$ is given results from the partial reflection assumption described above.

In several instances, large differences in σ_{I} values are found in computations made from different data planes of the same test. For example, $\sigma_{x\mathrm{I}}$ at 800 m during test P8 was computed as 151 m for the $z=1.5$ m data plane and as 67 m for the $\theta=130°$ data plane. Since the trivariate normal distribution requires equal values of $\sigma_{x\mathrm{I}}$ (or $\sigma_{y\mathrm{I}}$ or $\sigma_{z\mathrm{I}}$) regardless of the data plane employed in computation, such a distribution is not suggested. Even if the puffs were approximately trivariate normal at generation, it is felt that the effects of wind speed and direction shear deformed this distribution by the time the puffs traversed the 200 m arc.

Interest lies in the specification of absolute puff dimensions near the centroid of the puff where computed σ_{I} values were found to be higher. However, since measurements of puff dimensions were not always available near the centroid of the puff, the examination of the ratio of puff dimensions was felt to be an appropriate method of estimating near-centroid dimensions. It can be assumed that the ratio of dimensions ($\sigma_{z\mathrm{I}}/\sigma_{x\mathrm{I}}$, for instance) resulting from a slice through a puff will approximate that same ratio for a second slice parallel

TABLE 4. Measurements of puff dimensions.

Test	Ri	Data plane	200 m from source σ_{xI} (m)	σ_{yI} (m)	σ_{zI} (m)	σ_{yI}/σ_{xI}	σ_{zI}/σ_{xI}	800 m from source σ_{xI} (m)	σ_{yI} (m)	σ_{zI} (m)	σ_{yI}/σ_{xI}	σ_{zI}/σ_{xI}
P7	−0.16	$z=1$ 5m	32	9.9	(6.7)	0.30	—	75	54	—	0.72	—
		$\theta=114°$	30	—	5.4–7.2	—	0.18–0.24	84	(60)	9.8	—	0.12
P6	−0.04	$z=1.5$m	39	11.0	(6.4)	0.26	—	83	44	(11)	0.53	—
		$\theta=114°$	38	—	5.0–7.4	—	0.13–0.20	60	—	7.6	—	0.13
		$\theta=130°$	20	—	3.1	—	0.16	—	—	—	—	—
P3	−0.03	$z=1.5$m	33	12.6	—	0.38	—	112	28	(16)	0.25	—
		$\theta=114°$	37	(14.1)	4.9–6.1	—	0.13–0.16	64	—	9.2	—	0.14
P5	−0.02	$z=1.5$m	40	9.0	—	0.23	—	95	50	—	0.53	—
		$\theta=114°$	41	(9.2)	4.5–5.9	—	0.11–0.14	—	—	—	—	—
P8	0.07	$z=1.5$m	48	12.1	(6.3)	0.25	—	151	37	(16)	0.24	—
		$\theta=114°$	33	—	4.3	—	0.13	—	—	—	—	—
		$\theta=130°$	—	—	—	—	—	67	—	6.9	—	0.10
P2	0.13	$z=1.5$m	60	13.8	—	0.23	—	236	50	—	0.21	—

Figures in parentheses are estimates from measurements made outside the indicated data plane.

to the first. This assumption holds true for the one case in which computation from "parallel" slices was possible. At 200 m during test P6, the ratio of σ_{zI}/σ_{xI} was approximately 0.16 at both $\theta=114°$ and $\theta=130°$ (although σ_{xI} was found to be 38 m in the $\theta=114°$ plane and only 20 m in the 130° plane). The equal ratio assumption permits estimation of σ_I values near the puff centroid when only slices farther removed from the centerline are available for computation. For instance, from the 800 m data on test P3 listed on Table 4, it is assumed that if the vertical plane on which σ_{zI} was observed had been at a location where σ_{xI} was 112 m, instead of the observed 64 m, then σ_{zI} would have been about 16 m (i.e., 0.14×112), instead of 9.2 m. This estimated value of 16 m (and others similarly deduced) is entered in Table 4 in parentheses. Such estimates of σ_{yI} or σ_{zI} were made to accompany only the largest σ_{xI} values, and as such should reasonably closely indicate dimensions near the puff centroids.

These near-centroid dimensions are those graphed on Fig. 8. The shaded zones in the plots of crosswind and vertical dimensions vs distance are the range of measured values summarized in *Meteorology and Atomic Energy, 1968*. These data were originally reported by Smith and Hay (1961), Högström (1964), Cramer *et al.* (1964), Islitzer and Markee[2] and Taylor (1965). The ^{85}Kr puff data fall within the range of data generated from these earlier quasi-instantaneous releases.

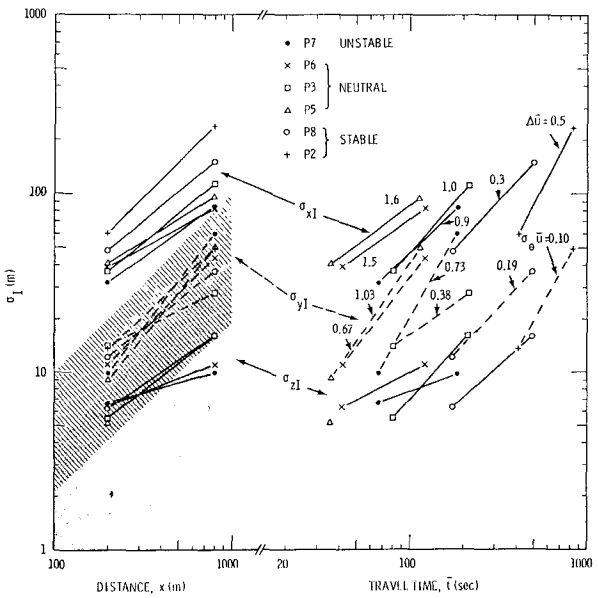

FIG. 8. Standard deviations of puff tracer distribution vs distance and travel time.

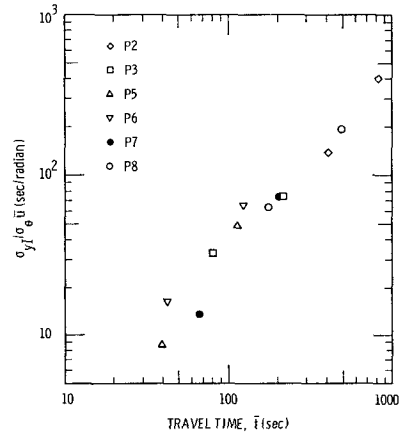

FIG. 9. Lateral standard deviation of puff (normalized to unit wind direction standard deviation and wind speed) as a function of travel time.

[2] Islitzer, N. F., and E. H. Markee, 1964: Puff diffusion measurements from reactor destructive tests. Paper presented at National Conference on Micrometeorology, Amer. Meteor. Soc., 13–16 October, Salt Lake City, Utah.

TABLE 5. Slope m in relationship $\sigma_I^2 \propto \bar{t}^m$.

Test	Ri	Travel time ($\bar{t}$) to 200 m (sec)	Travel time ($\bar{t}$) to 800 m (sec)	m for σ_{xI}^2	m for σ_{yI}^2	m for σ_{zI}^2
P7	−0.16	67	187	1.9	(3.5)	(0.74)
P6	−0.04	42	122	1.4	2.6	(1.0)
P3	−0.03	81	215	2.3	(1.4)	(2.2)
P5	−0.02	36	113	1.5	(3.0)	—
P8	0.07	176	493	2.2	2.2	(1.8)
P2	0.13	406	833	3.8	3.6	—

Figures in parentheses involve estimates listed in Table 4.

Table 4 and Fig. 8 indicate that $\sigma_{xI} > \sigma_{yI} > \sigma_{zI}$ regardless of stability. The left portion of Fig. 8 in which σ_I's are related to distance suggests that σ_{xI} is larger in stable atmospheres (tests P2 and P8) while there is minimal effect of atmospheric stability on σ_{yI} and σ_{xI}. However, when puff dimensions are considered as a function of time instead of distance, the stable tests imply smaller σ_I's than the neutral and unstable tests.

Slopes from the σ_{yI} vs distance curves range from 0.59 (neutral test P3) to 1.24 (unstable test P7). For stable test P8, σ_{yI} is proportional to $x^{0.81}$.

Fuquay *et al.* (1964) presented σ_y for plumes as a function of $\sigma_\theta \bar{u}$ and travel time. Values of $\sigma_\theta \bar{u}$ (from 1.5 m measurements) are noted adjacent to σ_{yI} curves on the right-hand portion of Fig. 8. The near perfect ordering of the curves with respect to $\sigma_\theta \bar{u}$ suggests the applicability of using this parameter in predicting σ_{yI}. Fig. 9, presenting $\sigma_{yI}/\sigma_\theta \bar{u}$ as a function of travel time, shows small stability effects.

Although the amount of data is admittedly small, there appears to be minimal correlation when σ_{yI} is considered as a function of time and σ_θ alone. Scatter diagrams of σ_{yI} vs σ_θ for a given distance also show little promise as predicting tools.

At the right in Fig. 8, the $\Delta\bar{u}$ figures listed with each σ_{xI} curve represent the differences (m sec^{-1}) between wind speeds measured at the 1.5 and 0.8 m elevations. The σ_{xI} vs time data stratify reasonably well with respect to this empirical parameter.

Examination of Table 4 reveals that σ_{yI}/σ_{xI} tended to decrease as stability increased. Also, σ_{zI}/σ_{xI} tended to decrease as stability increased, although this effect is not obvious at 800 m.

Table 4 shows that σ_{zI}/σ_{xI} always decreased slightly with distance (or time), while σ_{yI}/σ_{xI} decreased slightly for the stable tests, gave conflicting evidence for the neutral tests, but definitely increased with distance (or time) for the unstable test.

It is possible to comment on the puff dimensions from a more qualitative approach than in the preceding paragraphs. Note on Fig. 4 that, during both stable puff P8 and unstable puff P7, tracer was detected at 800 m while the tail of the distribution was still being observed at the 200 m arc. This situation was observed following all puff releases. Thus, without specifying magnitude of dosage or concentration, it can be stated with assurance that each puff stretched at least 600 m in the downwind direction while its centroid was about 500 m from the source point.

Since tracer was observed during all tests at the topmost elevation (10.7 m) on the 200 m towers, the vertical dimension at 200 m (again ignoring concentration magnitude) was always greater than 10.7 m. With one exception, each puff was observed at the topmost sensor (21.3 m) at an 800-m arc tower. The exception was during test P2, the most stable release, when the top of the puff was between 10.7 and 21.3 m at the 800 m distance.

Since it does take a finite time for a puff to pass an arc, the instantaneous width of the puff at an arc will be less than the width of the arc intercepted by the crosswind dosage due to the entire puff passage. For the unstable and neutral puffs, there was essentially no difference in these two widths. This was no doubt due to a great extent to the relatively high wind speeds and resulting short period of puff passage at an arc. During the two stable tests, when wind speeds were low, the effect of meander of the wind was seen much more clearly as the puff passed an arc. At 200 m during test P2, the largest detectable instantaneous dimension was about 84 m, while the dosage distribution embraced about 119 m. At 800 m, the instantaneous and dosage distributions embraced 196 m and 392 m, respectively.

Relative diffusion theory predicts that σ_{xI}^2, σ_{yI}^2 and σ_{zI}^2 increase initially as the third power of travel time. Table 5 indicates that the ^{85}Kr puffs generally grew at lesser rates. The rapid growth of σ_{yI} during test P2 can be attributed at least in part to the x-elongated puff being affected by an eddy larger than those in the inertial range for which the t^3 regime is predicted. The large slope of 3.8 for σ_{xI}^2 during P2 is likely a result of the particularly large vertical wind speed gradient observed near the surface during this stable experiment. Homogeneous turbulence conditions are assumed in development of the model embracing the t^3 regime.

The appeal of considering puff diffusion as a function of time rather than distance is exemplified in Table 6, where the data are derived from and amplify the interpretation of the curves of Fig. 8, but do include some rather large extrapolations. Although it must be ad-

TABLE 6. Averaged puff dimensions (m) vs distance and travel time.

Atmospheric stability	Observed wind speeds (m sec^{-1})	Distance from source: 200 m σ_{xI}	200 m σ_{yI}	200 m σ_{zI}	800 m σ_{xI}	800 m σ_{yI}	800 m σ_{zI}	Travel time: 1 min σ_{xI}	1 min σ_{yI}	1 min σ_{zI}	5 min σ_{xI}	5 min σ_{yI}	5 min σ_{zI}
Unstable to neutral	4 to 8	37	11	6	92	46	12	40	13	6	170	130	17
Stable	1 to 2	55	13	6	180	46	16	6	2	2	60	14	10

mitted that precisely the same numbers would not be generated by another attack on the Fig. 8 data, the basic pattern of Table 6 data would reappear. These tabulated data show that considering puff dimensions as a function of distance alone, σ_{zI} is greater in stable than in the less stable atmospheres and that stability has minimal effect on σ_{yI} and σ_{zI}. However, consideration of puff dimensions as a function of time gives the intuitively more appealing results at the right in Table 6, namely, that puff dimensions in stable atmospheres are smaller than they are in neutral or unstable atmospheres.

7. Summary

The following observations result from field measurements following eight instantaneous point source releases at ground level. Measurements were made near the puff centroid.

The effective speed and effective height of movement of puffs observed at the 1.5 m elevation increased with distance or time. The effect of atmospheric stability on this speed and height of movement was not obvious.

At the 1.5 m elevation, E_p, $\chi_{p\mathrm{CWI}}$ and χ_p increased with increasing stability. The measured peak exposures were in reasonable agreement with exposures from quasi-instantaneous sources reported by other researchers.

Regardless of stability, $\sigma_{xI} > \sigma_{yI} > \sigma_{zI}$ to a distance of 800 m. In the x-y plane, downwind elongation was more marked in stable atmospheres. In stable atmospheres, the downwind elongation continued during puff transport to 800 m. In an unstable atmosphere, puff dimensions in the x-y plane became more symmetrical during puff movement between 200 and 800 m. In the x-z plane, downwind elongation continued between 200 and 800 m regardless of stability.

Consideration of puff dimensions and concentrations as functions of travel time, rather than distance, revealed a more coherent picture in terms of the effects of atmospheric stability.

APPENDIX

Definition of Symbols

$\bar{u}_{1.5\mathrm{m}}$ mean wind speed at 1.5 m elevation during period of mean puff transport
θ azimuth
u_e effective transport speed
z_e effective transport height
Ri Richardson number for layer between 2.1 and 15.2 m
σ_u wind speed standard deviation at 1.5 m elevation during period of mean puff transport to 800 m
σ_θ wind direction standard deviation at 1.5 m elevation during period of mean puff transport to 800 m
σ_{I} standard deviation of concentration along a specified direction
x,y,z positions in a Cartesian coordinate system oriented so that the x axis is in the direction of the mean horizontal wind vector, the y axis is crosswind, and the z axis is vertical
Δx downwind distance moved by tracer in one 4.8-sec increment, equal to $u_e \Delta t$
Δy spacing between samplers along horizontal arc
χ concentration averaged over a 4.8-sec increment
χ_p peak χ
χ_{CWI} crosswind integrated concentration for a 4.8-sec increment; also defined as $\Sigma \chi \Delta y / Q$
$\chi_{p\mathrm{CWI}}$ peak χ_{CWI}
E exposure, a concentration time integral; also equal to $\Sigma \chi \Delta x / Q$
E_p peak or centerline exposure
M median of distribution of χ_{CWI} vs time
t elapsed time since puff generation
$\hat{t}$ time at mean of distribution of χ_{CWI} vs time at specific distance
Q amount of tracer released.

REFERENCES

Cramer, H. E., G. M. De Santo, R. K. Dumbauld, P. Morgenstern and R. N. Swanson, 1964: Meteorological prediction techniques and data system. Rept. GCA-64-3-G, Geophys. Corp. America, Bedford, Mass.

Fuquay, J. J., C. L. Simpson and W. T. Hinds, 1964: Prediction of environmental exposures from sources near the ground based on Hanford experimental data. *J. Appl. Meteor.*, **3**, 761–770.

Högström, U., 1964: An experimental study on atmospheric diffusion. *Tellus*, **16**, 205–251.

Ludwick, J. D., J. J. Lashock, R. E. Connally and P. W. Nickola, 1968: Automatic real time air monitoring of ^{85}Kr utilizing the 4096 memory of a multiparameter analyzer. *Rev. Sci. Instr.*, **39**, 853–859.

Nickola, P. W., and J. D. Ludwick, 1968: The measurement of particulate plume depletion in the atmosphere by com-

parison with an inert gaseous tracer. Pacific Northwest Laboratory 1967 Annual Report to USAEC Division of Biology and Medicine, Vol. II: Physical Sciences, Part 3: Atmospheric Sciences, BNWL-715, Part 3, 65–73. Battelle-Northwest, Richland, Wash. [Available from National Technical Information Service, NBS, U. S. Dept. of Commerce, Springfield, Va. 22151.]

——, J. V. Ramsdell, Jr., and J. D. Ludwick, 1970a: Detailed time-histories of concentrations resulting from puff and short-period releases of an inert radioactive gas: A volume of atmospheric diffusion data. BNWL-1272, Battelle-Northwest, Richland, Wash. [Available from National Technical Information Service, NBS, U. S. Dept. of Commerce, Springfield, Va. 22151.]

——, J. D. Ludwick and J. V. Ramsdell, Jr., 1970b: An inert gas tracer system for monitoring the real-time history of a diffusing plume or puff. *J. Appl. Meteor.*, **9**, 621–626.

Pacific Northwest Laboratory, 1970: Pacific Northwest Laboratory Annual Report for 1969 to the USAEC Division of Biology and Medicine, Vol. II: Physical Sciences, Part 1: Atmospheric Sciences. BNWL-1307–1, 6–10, 10–14, 21–25, 27–29. Battelle-Northwest, Richland, Wash. [Available from National Technical Information Service, NBS, U. S. Dept. of Commerce, Springfield, Va. 22151.]

Ramsdell, J. V., Jr., and W. T. Hinds, 1971: Concentration fluctuations and peak-to-mean concentration ratios in plumes from a ground-level continuous point source. *Atmos. Environment*, **5**, 483–495.

Smith, F. B., and J. S. Hay, 1961: The expansion of clusters of particles in the atmosphere. *Quart. J. Roy. Meteor. Soc.*, **87**, 82–101.

Taylor, J. H., 1965: Project Sand Storm, an experimental program in atmospheric diffusion. Environmental Research Papers, No. 134, Rept. AFCRL-65-649, Air Force Cambridge Research Laboratories.

U. S. Atomic Energy Commission, 1968: *Meteorology and Atomic Energy, 1968*. USAEC Division of Technical Information, 445 pages. [Available as TID-24190 from National Technical Information Service, NBS, U. S. Dept. of Commerce, Springfield, Va. 22151.]